

Therapeutically targeting cyclin D1 in primary tumors arising from loss of *Ini1*

Melissa E. Smith^a, Velasco Cimica^a, Srinivasa Chinni^a, Suman Jana^b, Wade Koba^b, Zhixia Yang^a, Eugene Fine^{b,c}, David Zagzag^d, Cristina Montagna^{a,c}, and Ganjam V. Kalpana^{a,c,1}

Departments of ^aGenetics and ^bNuclear Medicine and ^cCancer Center, Albert Einstein College of Medicine, Bronx, NY 10461; and ^dDepartment of Pathology and Neurosurgery, New York University, New York, NY 10016

Edited* by Stephen P. Goff, Columbia University College of Physicians and Surgeons, New York, NY, and approved November 29, 2010 (received for review November 17, 2009)

Rhabdoid tumors (RTs) are rare, highly aggressive pediatric malignancies with poor prognosis and with no standard or effective treatment strategies. RTs are characterized by biallelic inactivation of the *INI1* tumor suppressor gene. *INI1* directly represses *CCND1* and activates cyclin-dependent kinase (cdk) inhibitors p16^{INK4a} and p21^{CIP}. RTs are exquisitely dependent on cyclin D1 for genesis and survival. To facilitate translation of unique therapeutic strategies, we have used genetically engineered, *Ini1*^{+/-} mice for therapeutic testing. We found that PET can be used to noninvasively and accurately detect primary tumors in *Ini1*^{+/-} mice. In a PET-guided longitudinal study, we found that treating *Ini1*^{+/-} mice bearing primary tumors with the pan-cdk inhibitor flavopiridol resulted in complete and stable regression of some tumors. Other tumors showed resistance to flavopiridol, and one of the resistant tumors overexpressed cyclin D1, more than flavopiridol-sensitive cells. The concentration of flavopiridol used was not sufficient to down-modulate the high level of cyclin D1 and failed to induce cell death in the resistant cells. Furthermore, FISH and PCR analyses indicated that there is aneuploidy and increased *CCND1* copy number in resistant cells. These studies indicate that resistance to flavopiridol may be correlated to elevated cyclin D1 levels. Our studies also indicate that *Ini1*^{+/-} mice are valuable tools for testing unique therapeutic strategies and for understanding mechanisms of drug resistance in tumors that arise owing to loss of *Ini1*, which is essential for developing effective treatment strategies against these aggressive tumors.

SMARCB1 | *hSNF5* | genetically engineered mouse model | atypical teratoid/rhabdoid tumors

Rhabdoid tumors (RTs) are highly aggressive pediatric malignancies characterized by biallelic loss of the *INI1* tumor suppressor. RTs occur in various tissues, including the CNS, kidneys, and other soft tissues (1). Despite aggressive treatment, prognosis for children with RTs is poor. Mean survival with surgical intervention alone is 3 mo and with adjuvant chemotherapy and radiotherapy is 8 mo (2). Failure of RT therapies is possibly because they are based on treatment regimens derived from other tumor types. These regimens have been used partly because RTs were previously misclassified as Wilms tumor, choroid plexus carcinoma, germ cell tumor, ependymoma, glioblastoma, medulloblastoma, and primitive neuroectodermal tumor (1). Because RTs are unique, it is necessary to develop selective therapies effective against this tumor type. More than 95% of RTs arise owing to biallelic loss or inactivation of *INI1* (1, 3). Families that harbor an inherited, mutated/deleted allele of *INI1* suffer from RT predisposition syndrome and often develop rhabdoid and other tumors due to loss of heterozygosity (LOH) at the *INI1* locus (4). Various laboratories, including ours, have generated genetically engineered mouse models (GEMMs) that develop tumors due to LOH at the *Ini1* locus, thereby mimicking the etiology of human RTs. Loss of *INI1* is the major and sole critical alteration common to RTs, indicating that developing molecularly targeted therapies based on *INI1* function would help to effectively treat RTs and possibly other

tumors associated with *INI1* loss, such as schwannomatosis and epithelioid sarcoma.

INI1, a component of the SWI/SNF complex, induces G₀/G₁ arrest in RT cells by direct transcriptional repression of *CCND1* and activation of p16^{INK4a} and p21^{CIP} (5, 6). Our studies have revealed that RTs are exquisitely dependent on cyclin D1 for genesis and survival, and loss of *INI1* leads to derepression of cyclin D1 in primary mouse and human RTs (7–9). Genetic abrogation of *CCND1* eliminates RT formation in *Ini1*^{+/-} mice, and siRNA-mediated knockdown of *CCND1* is sufficient to induce G₀/G₁ arrest and apoptosis in RT cells (7). These studies, together with the fact that *INI1* activates CDKs p16^{INK4a} and p21^{CIP}, suggested that targeting cyclin D1 or the cyclin/cdk axis would be an effective means of inhibiting RT growth. Consistent with this, we have demonstrated that drugs that inhibit cyclin D1 and/or cyclins and cdk, such as fenretinide and flavopiridol, are effective in inhibiting RT growth with efficacy correlated with down-modulation of cyclin D1 (10, 11).

Although the above studies demonstrated that targeting cyclin D1 is effective in inhibiting RTs, they, like the majority of preclinical studies, are based on in vitro and xenograft models. Xenograft models are often poor predictors of therapeutic outcome in humans because tumors are most commonly derived from s.c. implantation of cells and are therefore homogeneous, ectopic, and developed in immunocompromised mice. In contrast to xenografts, GEMM-derived tumors are primary, autochthonous tumors that have appropriate tumor–stromal interactions and are in the setting of an intact immune system, both factors that can affect tumor progression and therapeutic response (12). Because tumors in GEMMs more closely mimic those found in humans, they are likely better predictors of therapeutic success, and preclinical testing using GEMMs may allow for more rapid translation of therapies into human trials (12). Another advantage is that variable response to drug treatment occurs owing to the heterogeneity of tumors in GEMMs, allowing for the study of mechanisms of drug resistance to improve treatment strategies.

Our goal was to use a GEMM for testing unique therapeutic strategies against RTs. *Ini1*^{+/-} mice, created in our laboratory, spontaneously develop CNS, face, and soft-tissue tumors due to LOH at the *Ini1* locus and exhibit many characteristics of human RTs (7). Despite the advantages of using GEMMs, one limitation is the difficulty associated with identifying and monitoring progression of primary tumors, which often form internally. Observation and quantification of such internal tumors for lon-

Author contributions: G.V.K. designed research; M.E.S., V.C., S.C., S.J., W.K., Z.Y., D.Z., and C.M. performed research; E.F. and C.M. contributed new reagents/analytic tools; M.E.S., W.K., C.M., and G.V.K. analyzed data; and M.E.S. and G.V.K. wrote the paper.

The authors declare no conflict of interest.

*This Direct Submission article had a prearranged editor.

¹To whom correspondence should be addressed. E-mail: ganjam.kalpana@einstein.yu.edu.

This article contains supporting information online at www.pnas.org/lookup/suppl/doi:10.1073/pnas.0913297108/-DCSupplemental.

itudinal studies requires a powerful, noninvasive imaging technique such as PET. Magnetic resonance imaging and computed tomography have been used to detect human RTs; however, PET is not yet routinely used for RTs (13).

We found that microPET accurately detects internal primary tumors spontaneously developed in *Ini1*^{+/-} mice. We then used microPET to follow the efficacy of flavopiridol, a pan-cdk inhibitor that inhibits RT growth in cell culture and xenograft tumor models (7, 11). We found that flavopiridol completely eliminates some well-established primary tumors in these mice, but we also observed flavopiridol-resistant tumors. We characterized one resistant tumor and found that flavopiridol resistance was intrinsic. Furthermore, FISH analysis indicated that the resistant tumor was aneuploid, and there was an increase in *CCND1* copy number. Our studies demonstrate the feasibility of using an *Ini1*^{+/-} GEMM for preclinical testing and PET for noninvasive imaging of primary tumors arising from loss of *Ini1*. The utility of this model to study mechanisms of drug resistance is also demonstrated.

Results

MicroPET Analysis of Primary Tumors Arising in *Ini1*^{+/-} Mice. Tumor visualization by microPET using 2-[(18)F]fluoro-2-deoxyglucose (¹⁸F-FDG) relies on the increased metabolic profile of tumor cells, involving increased expression of glucose transporters such as glucose transporter-1 (GLUT-1) (14). This allows detection of treatment response earlier than anatomic imaging modalities. GLUT-1 expression has been reported in CNS RTs, indicating that RTs could possibly be visualized by PET (15). To validate the use of GEMMs for therapeutic testing, three *Ini1*^{+/-} mice with visible tumors were subjected to microPET. The tumors in these mice were effectively identified by areas of ¹⁸F-FDG uptake. The visible mass on mouse D84 (Fig. 1*A1*) demonstrated a large area of ¹⁸F-FDG uptake ventrally below the left jaw (Fig. 1*A2* and *Movie S1*). Additionally, this mouse demonstrated three internal masses (Fig. 1*A2* and *Movie S1*). Two other mice (E66 and E7) presented with tumors on the face, which were evident in the digital photographs and PET images (Fig. 2*A1* and *A4* and *Movie S2* for mouse E7; and Fig. *S1 A1–A5* for mouse E66). Tumors identified by microPET were quantified by drawing regions of interest (ROIs) and by determining the standard uptake values (SUVs) as described in *Materials and Methods* and as illustrated in Fig. *S2*.

Fifteen additional mice with symptoms indicative of possible tumors, such as visible or palpable masses, alopecia, skin irritation, and behavioral abnormalities (head tilt, unusual gait, and leg clapping, which are possible indications of CNS tumors) were subjected to microPET to determine the accuracy and sensitivity of this detection method. One of these mice (D57) died during anesthesia before imaging was performed. Imaging of the remaining mice revealed the presence of tumors in 3 mice and no tumors in 11 mice. To ensure the accuracy of microPET, we subjected the 11 mice that did not show tumors to detailed necropsy and histology. The results of these analyses confirmed the lack of tumors in these mice and corroborated the microPET findings.

Effect of Flavopiridol on Growth of Primary Tumors Developed in *Ini1*^{+/-} Mice. After establishing that primary tumors can be imaged and quantified using PET, we sought to perform a pilot preclinical study using flavopiridol in a panel of six *Ini1*^{+/-} mice with tumors as indicated by microPET. These mice were treated with 7.5 mg/kg of flavopiridol once daily, 5 d/wk for 2 wk, followed by a 2-wk drug-free recovery period before a second course of treatment. Most mice were subjected to this regimen; however, a continuous 7-wk treatment schedule was used if the tumors did not respond to initial treatment. Mice were imaged using microPET before and after each course of treatment.

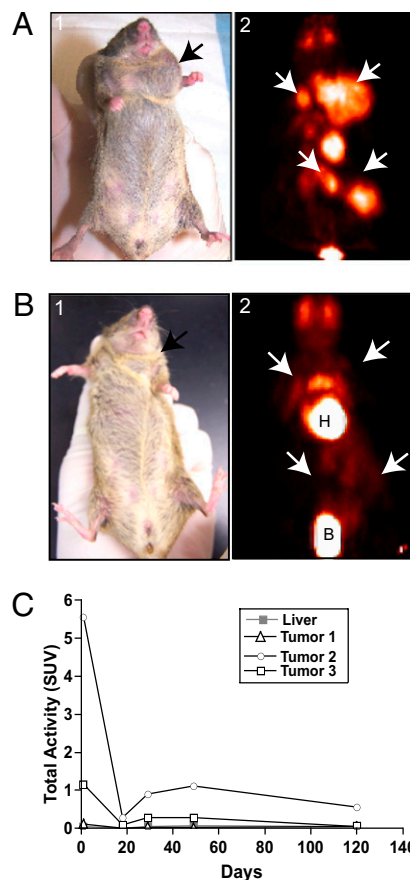


Fig. 1. PET analysis and flavopiridol-induced regression of a primary tumor in an *Ini1*^{+/-} mouse. (A) PET analysis of primary tumors arising in an *Ini1*^{+/-} mouse before treatment. (A1) Digital image of mouse D84, showing a neck mass; (A2) PET projection image of the same mouse, revealing increased ¹⁸F-FDG uptake, indicating the presence of multiple tumors within the neck and abdomen. (B) Digital and PET projection images of mouse D84 after round 1 of flavopiridol treatment. (B1) Digital image corresponding to the PET image in B2. Note the complete regression of all tumor masses in B2; the uptake seen above the heart is due to nonspecific muscle uptake. White arrows indicate the location of masses. H, heart; B, urinary bladder. (C) Graph showing SUVs of tumor masses. Liver is used as a measure of background uptake.

Of the mice undergoing treatment ($n = 6$), four survived until the study termination. Two of the surviving mice (D84 and M3) had complete responses to the flavopiridol regimen, whereas the other two (E7 and E66) had no response.

Mouse D84 (female, age 15.5 mo) had four tumors in the neck and abdomen, as indicated by ¹⁸F-FDG uptake (Fig. 1*A2* and *Movie S1*). Remarkably, all tumors regressed completely after one course of treatment with flavopiridol, as indicated by the loss of ¹⁸F-FDG uptake (Fig. 1*B2* and *Movie S3*). During the 2-wk treatment interruption one of the abdominal masses reappeared (Fig. *S3A4* and *Movie S4*). This mass, however, regressed again by the end of the second treatment course (Fig. *S3A5* and *Movie S5*). Mouse D84 was observed for 10 wk after the last treatment. No tumors reappeared during this period, indicating stable tumor-free survival for this mouse (Fig. *S3A6* and *Movie S6*). At the end of the study the mouse was necropsied, and no residual tumors were found, confirming the complete response. The microPET images were used to quantify the tumors, and plotting SUV vs. days from the start of the treatment clearly indicated a decrease in all tumor uptake values to background levels (Fig. 1*C*). The residual activity seen in Fig. 1*B2* and Fig. *S3 A4* and *A6* was likely due to uptake in muscle tissue.

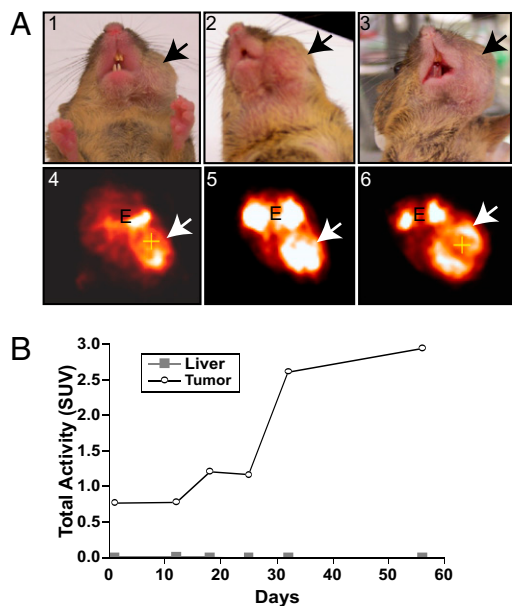


Fig. 2. PET analysis of an *Ini1*^{+/-} mouse with a primary tumor resistant to flavopiridol. (A) Digital and PET images of *Ini1*^{+/-} mouse E7 treated with flavopiridol. (A1 and A4) Images before treatment (day 1); (A2 and A5) Images after 2 wk of treatment with flavopiridol; (A3 and A6) Images after 7 wk of treatment with flavopiridol. White arrows indicate the location of the tumor. E, eyes. (B) Graph showing SUVs of the tumor. Liver is used as a measure of background uptake.

Another mouse, M3 (female, age 10 mo), was included in the study because of a behavioral abnormality: hind limb clamping when lifted by the tail (Fig. S3B1). MicroPET revealed intense ¹⁸F-FDG uptake in the cerebellum (Fig. S3B2). This mouse was treated with the same schedule as mouse D84, with two rounds of treatments and 2 wk of treatment interruption between each round. After the first round of flavopiridol treatment, microPET imaging showed that tracer uptake within the brain had returned to background levels. Subsequent images after the second round of treatment indicated that the tumor did not recur (Fig. S3 B3–B5). The mouse was observed for 4 wk after the last treatment before necropsy and histopathology. No trace of tumor was found after the detailed necropsy, which further confirmed complete regression of the tumor.

In contrast to the above two cases, tumors in mice E7 (female, age 17 mo) and E66 (female, age 19 mo) showed no response to flavopiridol. Weekly imaging of both mice demonstrated continuous tumor growth despite 7 wk of uninterrupted treatment (mouse E7: compare Fig. 2 A4, A5, and A6; Movies S2, S7, and S8). Determination of SUVs during the treatment verified these findings (Fig. 2B). The microPET images and histopathology of the other resistant tumor from mouse E66 before treatment are shown in Fig. S1 A and B.

Of the remaining two mice included in this study, D56 (male, age 16 mo) and L68 (male, age 12 mo) died shortly after treatment initiation. It is unclear at this point whether these mice died of progressive disease or from flavopiridol-associated toxicities.

Histological and Ultrastructural Characterization of a Flavopiridol-Resistant Tumor. The heterogeneity of GEMM tumors leads to variable treatment responses, similar to what is observed in humans, allowing for GEMMs to be better predictors of treatment efficacy. Thus, GEMMs are valuable tools to study drug resistance. We characterized the resistant tumor from mouse E7 to understand the reasons for resistance. The tumor was used to establish a primary cell line and orthograft tumors in SCID mice.

Both the primary tumor isolated from E7 and the orthograft of E7 (xE7) were characterized by histopathology and immunohistochemistry (IHC) (Fig. S4). The results indicated that the tumor was an anaplastic sarcoma containing sheets of loosely interlacing spindle cells and scattered rhabdoid cells (Fig. S4 A–C). The presence of spindle cells indicates similarity to other tumor types, such as malignant peripheral nerve sheath tumor (MPNST) or schwannomatosis. In recent years, loss of *INI1* has been noted in tumors other than RTs, such as schwannomatosis and epithelioid sarcoma (16, 17). Furthermore, cooccurrence of schwannomatosis and RT has been noted in a family that carries a germline *INI1* mutation (18). For these reasons, we surmised that E7's tumor could be a variant of RTs, and its resistance to flavopiridol may stem from this fact.

To establish the nature of the tumor, we performed IHC using a panel of antibodies on paraffin sections of normal brain, primary resistant tumor (E7), and an orthograft-passaged tumor, xE7 (Fig. S4D). *Ini1* staining was negative in the resistant tumor cells, a primary characteristic of RTs (Fig. S4 D10 and D18). Cyclin D1 and smooth muscle actin (SMA), often overexpressed in RTs, were highly expressed within the resistant tumor cells (Fig. S4 D11, D12, D19, and D20). Other markers, sometimes overexpressed in RTs, such as glial fibrillary acidic protein (GFAP), synaptophysin, and cyokeratin, were found to be negative within the resistant tumor (Fig. S4 D13–15 and D21–23). Because these markers are not consistently expressed in RTs, this was inconclusive for diagnosis. S100, expressed in MPNST and schwannomatosis, was also found to be negative within the resistant tumor (Fig. S4 D16 and D24). This IHC panel helped characterize the resistant tumor and revealed that the orthograft-passaged tumor maintained characteristics of the primary tumor.

Ultrastructural analysis using transmission electron microscopy (TEM) has demonstrated that RT cells are characterized by the presence of whorls of cytoplasmic filaments, an eccentric nucleus, and one prominent nucleolus (19). To determine whether the resistant tumor cells retain these characteristics, a comparative ultrastructural analysis of MON RT cells and flavopiridol-resistant E7 cells was carried out. TEM of both cell types showed the distinct characteristics of RTs, indicating that the resistant tumor is likely rhabdoid (Fig. 3 A and B).

Effect of Drugs on the Survival of Resistant Tumor Cells in Culture.

The mechanism of resistance could be due to a genetic alteration within the tumor cells (intrinsic mechanism) or due to changes at the organismal level; either in the tumor environment, tumor location, or in drug metabolism (extrinsic mechanism). Drug resistance associated with an extrinsic mechanism will likely be lost when tumor cells are isolated from the mouse and grown in culture. Therefore, we isolated cells from the primary tumor and passaged them in culture to determine their sensitivity to drugs in vitro. To establish the purity of the culture, we examined the cells by TEM for the presence of cytoplasmic filamentous whorls, a characteristic of RTs (19), and found that >60% of the cells were clearly rhabdoid.

We observed that E7 cells exhibited limited proliferation, and after four passages in culture, underwent senescence. Therefore, we used early passages for in vitro studies. Past studies from our laboratory demonstrated that flavopiridol (11) and fenretinide (10) are effective in inhibiting the growth of RT cell lines. We compared the efficacy of these drugs in E7 cells with that in two RT cell lines, MON and G401 (*IC*₅₀ for flavopiridol ≈150 and 200, respectively), which are differentially sensitive to these drugs. We found that E7 cells are markedly resistant to both drugs (Fig. 4 A and B). These in vitro studies therefore demonstrated that the mechanism of drug resistance is an intrinsic mechanism.

The efficacy of both flavopiridol and fenretinide in RT cells is correlated with their ability to down-regulate cyclin D1 (10,

there is amplification of the *CCND1* locus (more than two copies per cell) in the majority of tumor cells.

To determine whether amplification of *CCND1* exceeds that of the another gene on the same chromosome, we first carried out quantitative PCR (qPCR) analysis using DNA from normal liver and E7 tumor, comparing the dosage of *CCND1* with that of protein kinase $c\text{-}\gamma$ (*PRKCC*), a gene proximal to the centromere on chromosome 7 or to that of ribosomal protein S18 gene (*RPS18*), a housekeeping gene (Fig. 4E). The dosage of *CCND1* was increased approximately threefold in tumor cells when normalized to either that of *PRKCC* or *RPS18* (Fig. 4E). Karyotype analysis of E7 resistant tumor cell metaphase spreads indicated that cells were variably aneuploid (Fig. 4E and Fig. S7 A and B) and had copy numbers of *CCND1* exceeding the expected ploidy in most cells (Fig. 4F, fifth column). Further analysis indicated that *CCND1* mapped not only to the extranumerary copies of mouse chromosome 7 (gain reflecting whole chromosome aneuploidies) but was also amplified owing to genomic rearrangements with chromosome 19 (Fig. S7 B and C). These results indicated that the increase in cyclin D1 levels in the E7 tumor is likely due to increased copy number of *CCND1* locus.

Discussion

To facilitate the translation of unique therapeutic strategies, we have used an *Ini1*^{+/-} GEMM for preclinical studies. We demonstrated that microPET detects primary tumors arising in these mice with a high degree of specificity. Furthermore, microPET allows for quantification of tumor response, such that longitudinal therapeutic efficacy studies can be conducted. To fully validate this model for preclinical testing, we carried out a pilot study using flavopiridol. Overall, we found that response to flavopiridol was variable and represented an all-or-none phenomenon. Of the six mice selected for treatment, four survived to receive full courses of treatment, and two died during treatment. Of the four surviving mice, two showed complete tumor regression, and two demonstrated resistance to therapy with no response. It is interesting to note that there were no partial responses to flavopiridol. This may reflect the property of flavopiridol, whereby achieving a threshold concentration is critical for its function and below this concentration it is ineffective. These findings demonstrate the importance of using GEMMs for preclinical studies; despite the common origin of these tumors, other genetic variations within tumors and between animals result in different responses to chemotherapeutics.

The response seen in mouse D84 is dramatic: four well-established tumors regressed completely after one round of flavopiridol treatment. A second mouse, mouse M3, presented with a behavioral abnormality, and microPET showed intense uptake near the cerebellum. This uptake was stably reduced to background levels after one round of flavopiridol treatment. Because RTs are aggressive and have very poor prognosis any success in completely eliminating these tumors in preclinical models is significant, and these results may lead to improved therapeutic strategies.

Ini1^{+/-} GEMMs more closely mimic RT predisposition syndrome, and a recent study found the occurrence of RTs and schwannomatosis in one family due to the same inherited mutation in *INI1* (18). It may therefore be important to consider the age of onset and characteristics of the tumors because germline *INI1* mutations are capable of inducing several distinct malignancies that will likely respond differently to therapies.

Ini1^{+/-} mice also are valuable for the study of resistance to unique therapeutic strategies. In this study we have isolated a mouse RT resistant to flavopiridol. Cells from this tumor expressed threefold higher levels of cyclin D1 than flavopiridol-sensitive RT cells. Increased protein levels were correlated to increased *CCND1* copy number in tumor cells that was a result of aneuploidy and genomic rearrangement. *CCND1* was found both

on extranumerary chromosome 7 and on chromosome 19. Additionally, concentrations of flavopiridol sufficient to completely down-modulate cyclin D1 in other RT cells were not sufficient to do so in resistant E7 cells. These results suggest a role for increased *CCND1* copy number in inducing resistance to flavopiridol. Further studies are required to establish the nature of genomic rearrangements and a definitive role of cyclin D1 in promoting drug resistance in RTs. Nevertheless, our results are in line with the previous observation that cyclin D1 is essential for survival and genesis of RTs and that the efficacy of flavopiridol correlated with down-modulation of cyclin D1 (7, 10, 11).

Interestingly, higher concentrations of flavopiridol and fenretinide induced cytotoxicity in E7 resistant cells in vitro (Fig. 4 A and B), indicating that perhaps administering higher amounts of flavopiridol may be effective in inhibiting these resistant tumors. Unfortunately, flavopiridol at concentrations higher than 7.5 mg/kg is toxic to mice and hence we could not test this hypothesis in vivo. We believe that developing more tolerable derivatives of flavopiridol or combining flavopiridol with other drugs that can act synergistically to lower its IC₅₀ will be valuable for treating these resistant tumors.

Flavopiridol may be effective in eliminating not only RTs but other tumors that have lost *INI1* and express moderate levels of cyclin D1. RTs and other tumors that express higher levels of cyclin D1 could be treated with flavopiridol in combination with other drugs. Further analysis of such drug combinations that improve the efficacy of flavopiridol may provide a much-needed therapeutic strategy for RTs, which are notoriously resistant to current treatment regimens.

Materials and Methods

Mice. Breeding, maintenance, and treatment of mice were carried out in accordance with the Albert Einstein College of Medicine Institutional Animal Care and Use Committee (IACUC), accredited by Association for Assessment and Accreditation of Laboratory Animal Care International and approved by the National Institutes of Health Office of Laboratory Animal Welfare, and inspected by the United States Department of Agriculture Animal and Plant Health Inspection Service. At study termination, all mice were humanely killed according to IACUC protocols. C57BL/6J mice carrying *Ini1*^{+Δexons6,7} mutations (denoted as *Ini1*^{+/-}) were generated in our laboratory as previously described (7). SCID mice used for orthografting were purchased from Taconic and maintained as previously described (11).

PET Imaging and Quantitation of Tumors. Mice were fasted for 3 to 4 h, then anesthetized with isofurane gas and injected with 200–300 μCi of ¹⁸F-FDG via tail vein. After injection, 60 min was allowed for adequate uptake of ¹⁸F-FDG throughout the body. For PET scanning, the mouse was placed at the center of the scanner's field of view (R4 scanner; Concord) and subjected to a 10-min transmission scan (using a ⁵⁷Co source) followed by a 10-min emission scan. Any mouse suspected to have a brain tumor (either by symptoms or from review of the whole body image) underwent additional scans centered on the brain. Mice were recovered from anesthesia for 10–15 min after the scan. Images were reconstructed using the ordered subsets expectation maximization protocol with attenuation and scatter corrections and by applying a zoom factor of either 2 or 5 for body images or brain images, respectively.

Tumor masses were quantified by calculating SUVs using ASIPro software (CTI Molecular Imaging). Using ASIPro, 3D ROIs were selected to encompass the region of increased ¹⁸F-FDG uptake (representing the tumor mass). To minimize partial-volume effects arising because the activity-containing volume (e.g., tumor) is below the intrinsic resolution of the scanner, ROIs were consistently drawn to enclose a 30- to 40- μL volume. SUVs of the ROIs were calculated by the software using a ratio of the radioactivity concentration within the ROIs at a given time to the injected dose of radiation and divided by the body weight of the mouse. A ROI was also selected for the liver to determine background ¹⁸F-FDG uptake.

In Vivo Drug Treatment. Solutions of 1 mg/mL flavopiridol were prepared weekly in 0.9% saline (AmTech) containing 0.1% DMSO, heated to 37 °C, vortexed, and stored at –80 °C. The solution was again heated to 37 °C and

vortexed to dissolve the drug completely before i.p. injection at a final dose of 7.5 mg/kg according to the weight of each mouse.

Isolation of a Primary Cell Line from Flavopiridol-Resistant Mouse E7 Tumor. Immediately after killing, the tumor was resected, dipped in 70% ethanol, and placed in α MEM supplemented with 50 U/mL penicillin and 50 μ g/mL streptomycin (P/S). The tumor was diced using sterile scalpels and centrifuged at $67 \times g$ for 5 min. The supernatant was removed, and pellet was resuspended in 10 mL of α MEM medium supplemented with P/S and 10% FBS. The suspension was then plated into several wells of a six-well plate and incubated at 37 °C at 5% CO₂. Medium was changed twice per week, and when adherent cells reached 60% confluency they were passaged. Cells grown in α MEM were easily adapted to DMEM supplemented with P/S, 2 mM L-glutamine, and 10% FBS for further studies.

Establishment of Orthografted Tumors. The primary tumor mass resected from the mouse was disaggregated by dicing in α MEM medium and by passing through a 19G needle. Tumor suspension (300 μ L) was injected s.c. into the flank of SCID mice. Before reaching 300 mm³, tumors were passaged into new SCID mice. Cells were isolated from orthografted tumors in the same manner as from the primary tumor for in vitro studies.

Cell Culture and Drug Treatments. The *INI1*-null RT cell lines, MON (3) and G401 (American Type Culture Collection), were cultured as previously described (11). Cells isolated from the flavopiridol-resistant tumor (E7) and an orthograft-passaged tumor (xE7) were cultured in DMEM supplemented with 10% FBS, P/S, and 2 mM L-glutamine. Flavopiridol and fenretinide stock solutions were prepared as previously described (10, 11). Working solutions (3 μ M flavopiridol, 50 μ M fenretinide) and serial dilutions were prepared by diluting the stocks with culture medium, such that the final concentrations of DMSO and ethanol were constant in all wells of each assay.

Drug Effects on Cell Survival in Vitro. Methyl-tetrazolium salt assays were carried out as previously described (11).

Histopathology and Immunohistochemical Analysis. Paraffin sections (5 μ m) were deparaffinized in xylene followed by graded alcohols and stained using H&E or subjected to IHC. For IHC, antigen retrieval was performed in 10 mM sodium citrate buffer (pH 6.0) at 96 °C for 30 min. Endogenous peroxidase activity was blocked using 0.3% hydrogen peroxide. The subsequent steps were based on a standard protocol (11). Primary antibodies used were α -INI1 at 1:100 (BD Transduction Laboratories, #612110), α -cyclin D1 (#18-0220; at 1:100; Zymed), α -SMA (#A2547; at 1:1,000; Sigma), α -GFAP (#Z00334; at 1:1,000; Dako), synaptophysin (#1485-1; at 1:250; Epitomics), α -pan-cytokeratin (#C2562; at 1:300; Sigma), and α -S100 (#MS-296; at 1:500; Thermo Scientific) antibodies.

Transmission Electron Microscopy. Cells were fixed with 2.5% glutaraldehyde in 0.1 M sodium cacodylate buffer at room temperature. Cells were postfixed with 1% osmium tetroxide followed by 2% uranyl acetate, dehydrated through a graded series of ethanol, and embedded in LX112 resin (LADD Research Industries). Ultrathin sections were cut on a Reichert Ultracut UCT and stained with uranyl acetate followed by lead citrate. Images were collected using a JEOL 100 CXII or JEOL 1200EX electron microscope at 80 kv.

Immunoblot Analysis. Chemiluminescence detection was achieved using SuperSignal West Pico or Femto Chemiluminescence Substrate (#34080 or #34095; Pierce) and by using α -INI1 (20), α -cyclin D1 (#MS-210; Thermo Scientific), and α -GAPDH (#MAB374; Chemicon International) antibodies.

FISH and Genomic Analysis. BAC clones specific to *CCND1* locus (RP24-186B2, chr7:152,062,597-152,230,717) and to the 3' end flanking region (RP24-316N16, chr7:152,331,071-152,515,971) were obtained from Bac/Pac Resources Children's Hospital and Research Center at Oakland, CA (<http://bacpac.chori.org/vectorsdet.htm>). DNA isolation and labeling and hybridization and detection were performed as previously described (21). Labeled probes (*CCND1* locus-specific probe in Spectrum Orange and 3' end flanking region in biotin detected Alexa 647) were tested to ensure unique mapping to the locus of interest on mouse WT C57B6 female metaphase spleen preps (Fig. S7A1). Tumor cells were grown to 40–60% confluency in four-well chamber slides (#354104; BD Falcon), fixed in ice-cold methanol for 10 min, and pretreated for removal of cytoplasm [pepsin (Sigma), 50 μ g/mL for 10 min,] before FISH analysis. For performing FISH on paraffin sections, 4- μ m-thin tumor sections were incubated overnight on a slide warmer at 60 °C, deparaffinized in xylene, and pretreated with a protease solution (Vysis, Abbott Molecular) at 37 °C for 20 min, as previously described (21). Chromosome counts for ploidy and full karyotype were carried out by the expert author C.M., on the basis of inverted DAPI images using the BandView application of the ASI acquisition system (Applied Spectral Imaging). Quantitative PCR analysis was carried out using primers for mouse *CCND1* (5': AGTCGGGGAGGGGTGCCTTC; 3': TGCA-GAATGGGGCACAAGC) and mouse *PRKCC* (5': TGCCGGGGTGTGCTTTCTG; 3': GGTGGACGGCGTAGGAGGA).

ACKNOWLEDGMENTS. We thank Drs. B. Birshstein, I. D. Goldman, and S. Horwitz at Albert Einstein College of Medicine (AECOM) for critically reading the manuscript; Drs. S. Horwitz and S. Mani at AECOM for useful discussions; Dr. R. S. Sellers at AECOM for pathology and immunohistochemistry assistance; Dr. D. Colevas at the National Cancer Institute Cancer Therapy Evaluation Program (NCI CTEP, Bethesda, MD) for providing flavopiridol; and Dr. Smith at CTEP NCI for providing fenretinide. This work was supported by American Cancer Society Grant RSG CCG-10493, the Children's Tumor Foundation, an AECOM Cancer Center pilot grant, and philanthropic funding (Amini Foundation) (to G.V.K.); and National Institute of General Medical Sciences Grant T32 GM 007491 (to M.E.S.). G.V.K. is a Mark Trauner faculty scholar and a recipient of the Irma T. Hirsch Career Scientist Award.

- Biegel JA (2006) Molecular genetics of atypical teratoid/rhabdoid tumor. *Neurosurg Focus* 20:E11.
- Tekautz TM, et al. (2005) Atypical teratoid/rhabdoid tumors (ATRT): Improved survival in children 3 years of age and older with radiation therapy and high-dose alkylator-based chemotherapy. *J Clin Oncol* 23:1491–1499.
- Versteegje I, et al. (1998) Truncating mutations of hSNF5/INI1 in aggressive paediatric cancer. *Nature* 394:203–206.
- Sévenet N, et al. (1999) Constitutional mutations of the hSNF5/INI1 gene predispose to a variety of cancers. *Am J Hum Genet* 65:1342–1348.
- Chai J, Charboneau AL, Betz BL, Weissman BE (2005) Loss of the hSNF5 gene concomitantly inactivates p21CIP/WAF1 and p16INK4a activity associated with replicative senescence in A204 rhabdoid tumor cells. *Cancer Res* 65:10192–10198.
- Zhang ZK, et al. (2002) Cell cycle arrest and repression of cyclin D1 transcription by INI1/hSNF5. *Mol Cell Biol* 22:5975–5988.
- Tsikitis M, Zhang Z, Edelman W, Zagzag D, Kalpana GV (2005) Genetic ablation of Cyclin D1 abrogates genesis of rhabdoid tumors resulting from Ini1 loss. *Proc Natl Acad Sci USA* 102:12129–12134.
- Fujisawa H, Misaki K, Takabatake Y, Hasegawa M, Yamashita J (2005) Cyclin D1 is overexpressed in atypical teratoid/rhabdoid tumor with hSNF5/INI1 gene inactivation. *J Neurooncol* 73:117–124.
- McKenna ES, et al. (2008) Loss of the epigenetic tumor suppressor SNF5 leads to cancer without genomic instability. *Mol Cell Biol* 28:6223–6233.
- Alarcon-Vargas D, et al. (2006) Targeting cyclin D1, a downstream effector of INI1/hSNF5, in rhabdoid tumors. *Oncogene* 25:722–734.
- Smith ME, et al. (2008) Rhabdoid tumor growth is inhibited by flavopiridol. *Clin Cancer Res* 14:523–532.
- Sharpless NE, Depinho RA (2006) The mighty mouse: Genetically engineered mouse models in cancer drug development. *Nat Rev Drug Discov* 5:741–754.
- Packer RJ, et al. (2002) Atypical teratoid/rhabdoid tumor of the central nervous system: Report on workshop. *J Pediatr Hematol Oncol* 24:337–342.
- Mamede M, et al. (2005) [¹⁸F]FDG uptake and PCNA, Glut-1, and Hexokinase-II expressions in cancers and inflammatory lesions of the lung. *Neoplasia* 7:369–379.
- Loda M, Xu X, Pession A, Vortmeyer A, Giangaspero F (2000) Membranous expression of glucose transporter-1 protein (GLUT-1) in embryonal neoplasms of the central nervous system. *Neuropathol Appl Neurobiol* 26:91–97.
- Hulsebos TJ, et al. (2007) Germline mutation of INI1/SMARCB1 in familial schwannomatosis. *Am J Hum Genet* 80:805–810.
- Modena P, et al. (2005) SMARCB1/INI1 tumor suppressor gene is frequently inactivated in epithelioid sarcomas. *Cancer Res* 65:4012–4019.
- Swensen JJ, et al. (2009) Familial occurrence of schwannomas and malignant rhabdoid tumour associated with a duplication in SMARCB1. *J Med Genet* 46:68–72.
- Bambakidis NC, Robinson S, Cohen M, Cohen AR (2002) Atypical teratoid/rhabdoid tumors of the central nervous system: Clinical, radiographic and pathologic features. *Pediatr Neurosurg* 37:64–70.
- Cheng SW, et al. (1999) c-MYC interacts with INI1/hSNF5 and requires the SWI/SNF complex for transactivation function. *Nat Genet* 22:102–105.
- Montagna C, et al. (2003) The Septin 9 (MSF) gene is amplified and overexpressed in mouse mammary gland adenocarcinomas and human breast cancer cell lines. *Cancer Res* 63:2179–2187.